Korean J. Chem. Eng., **16**(5), 670-676 (1999)

Hydrodynamics Study of Two Different Inverse Fluidized Reactors for the Application of Wastewater Treatment

Ho Suk Choi† **and Min-Su Shin**

Department of Chemical Engineering, Chungnam National University, Taejon 305-764, Korea
(*Received 14 April 1999 • accepted 7 June 1999*)

Abstract–We investigated the hydrodynamic characteristics of two types of inverse fluidized bed reactors having different driving force for fluidization: aeration and centrifugal force. In the first reactor, only an upward gas flow allows floating low-density polyethylene beads to sink down into liquid phase and to be uniformly distributed over the entire column. The gas velocity at which the solid concentration is uniform throughout the bed expansion decreases with increasing particle loads. In the second reactor, the particle loads do not greatly affect the critical rotating velocity for the homogeneous distribution of solid particles while the geometry of reactor spacing and the type of impeller are more important for the distribution of particles. For the application of wastewater treatment, the inverse fluidized bed with aeration was found to be more efficient than the second type of reactor.

Key words : Inverse Fluidization, Hydrodynamics, Biocarrier, Wastewater Treatment, Centrifugal Force

INTRODUCTION

Biotechnology has been greatly improved in the field of the immobilization of microbes on the solid substrate [Yoon et al., 1982; Koh and Chang, 1979]. This technique is better than the immobilization of enzymes because it is stable as well as economic [Frida and Kolot, 1981]. The immobilization of microbes allows us to constantly provide enzymes from immobilized microbes. In order to effectively apply this technique to industry, the development of suitable biocarriers is very important. The biocarriers for the immobilization of microbes are divided into two kinds: organic and inorganic materials. In this study, we choose polyethylene beads as biocarriers since the polyethylene is used in various applications due to its low cost, ready availability and resistance to chemicals and harsh environments. Also, the high specific modulus and strength of polyethylene make it a good candidate for acting as a reinforcing component in laminates/composites. One of the major markets for polyethylene is the packaging industry where it is used directly or in the form of laminates with aluminum foil, paper, etc. [Dibyendu et al., 1997]. However, polyethylene has a hydrophobic surface property which is not good for the immobilization of microbes. Thus, we modified the surface property of the polymer substrate from hydrophobic to hydrophilic by treating the polyethylene surface with chlorosulfonic acid. This chemical modification not only changes the hydrodynamic characteristics of particles in fluid phase but also increases the retention capacity of microbes on the solid biocarriers [Yang et al., 1997].

To effectively use the biocarriers with density lower than that of liquid for the application of wastewater treatment, the concept of inverse fluidization is needed [Wild et al., 1982; Lee and De Lasa, 1987; Nikolov and Karamanev, 1987; Fan, 1989; Roustan et al., 1993; Bastoul et al., 1996; Lee et al., 1989]. Such a system can be operated with downward flow of the liquid counter to the net upward buoyancy force on the particles. The gas flow is upward, counter to the liquid flow and bed expansion can be supported by either the (downward) liquid phase, the (upward) gas bubbles, or both [Fan et al., 1982; Krishnaiah et al., 1993]. In this study, we investigated the hydrodynamic characteristics of two different inverse fluidizations: one is using upward gas bubbles and the other is using downward liquid flow due to centrifugal force. So far, however, only a limited number of studies are available on these inverse fluidized reactors [Fan et al., 1982; Hinh et al., 1992; Krishnaia et al., 1993; Legile et al., 1988; Comte et al., 1997]. Thus, the primary objective of this study is to independently characterize the hydrodynamic behaviors of two inverse fluidizations. The secondary objective is to compare the hydrodynamic performances of the two reactors for the application of wastewater treatment.

EXPERIMENTALS

We studied two different reactors: One (Fig. 1) is the inverse fluidized reactor using aeration and the other (Fig. 2) is the inverse fluidized reactor using centrifugal force. In Fig. 1, the air from the bottom air distributor makes water recirculate in the bed and biocarriers fall down. In this apparatus with a transparent acrylic column of 10.7 cm inner diameter and 50 cm height, hydrodynamic experiments were mainly performed. Air, water and biocarriers were used as the gas, liquid and solid phases, respectively. We used a ceramic material as a gas distributor. Equally spaced pressure taps were mounted on the column wall from the sparger up and connected to water manometers. To prevent solid particles from entering into the pressure measurement lines, a polymeric screen was attached to the tip of each pressure tap.

†To whom correspondence should be addressed.
E-mail : hchoi@hanbat.chungnam.ac.kr

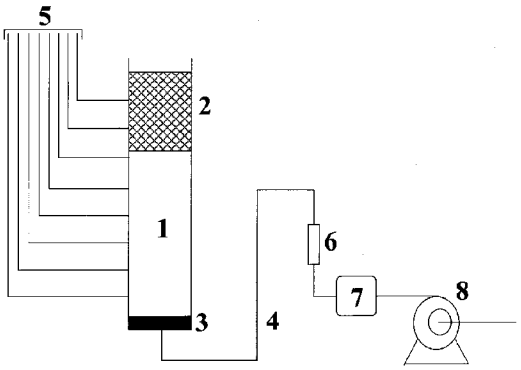

Fig. 1. Schematic diagram of the inverse fluidized reactor using aeration.

1. Column
2. Solid particles
3. Air distributor
4. Air inlet
5. Pressure taps
6. Rotameter
7. Regulator
8. Compressor

We used chemically treated low density polyethylene (LDPE) beads as biocarriers. The shape of biocarriers is oblate and the average diameter is 3.86 mm, thickness of 2 mm, average density 0.93 g/cm^3; sphericity 0.93; void fraction 0.386. We used three steps for modifying the surface of polyethylene beads. First, polyethylene beads were mixed with 10 mM-ferric chloride solution at 30 °C for 3 hours. The pretreated beads were water washed and vacuum dried for 30 min. Then, we etched polyethylene beads in chlorosulfonic acid solution [$ClSO_3H$: CCl_4=2 : 1(w/w)] with stirring for 4 hours at room temperature. After etching polyethylene beads were water-washed for at least 15 min and vacuum-dried over 1 hr.

In the apparatus represented in Fig. 2, we measured a critical mixing velocity for the minimum fluidization of biocarriers at different conditions such as the position of impeller and the particle loading. The reactor is made of Pyrex and the temperature is controlled by warm water circulating through the jacket. The reactor with an inner diameter of 16 cm and the height of 41.3 cm has an inner tube with an inner diameter of 10.7 cm and a height of 28 cm. The impeller is an anchor type with the dimensions shown in Fig. 2. In this experiment, we used both

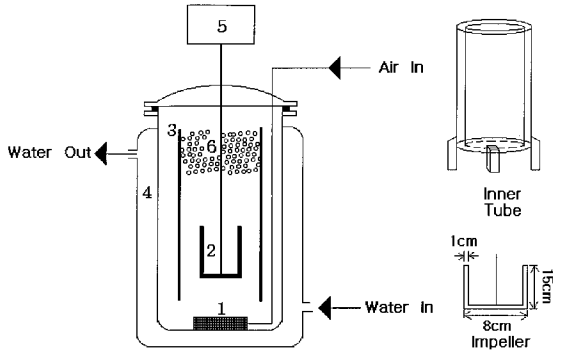

Fig. 2. Schematic diagram of the inverse fluidized reactor using centrifugal force.

1. Air distributor
2. Anchor type stirrer
3. Inner
4. Water jacket
5. Motor
6. Biocarriers

untreated and treated LDPE beads. The untreated and treated LDPE beads have a density of 0.903 g/cm^3 and 0.93 g/cm^3, respectively. We also conducted experiments in the reactor without the inner tube.

RESULTS AND DISCUSSIONS

1. Hydrodynamics of the Inverse Fluidized Reactor using Aeration

First, we obtained the gas holdups of the bubble column (without solid particles) in the first reactor (Fig. 1) to check the performance of the apparatus and compared the values obtained from the observation of liquid level rise with the values calculated from the pressure drop measurements (Fig. 3). The ε_G was calculated from Eqs. (1) and (2) after setting ε_S=0. Fig. 4 shows good agreement between the measured and calculated values and confirms the accuracy of the manometer. The observed result was obtained from the height of bed expansion due to aeration. Then, we obtained the average phase holdups in the three-phase fluidized bed from the following equations:

$$-\frac{dP}{dz}=(\varepsilon_G\rho_G+\varepsilon_L\rho_L+\varepsilon_S\rho_S)g. \quad (1)$$

$$\varepsilon_G+\varepsilon_L+\varepsilon_S=1. \quad (2)$$

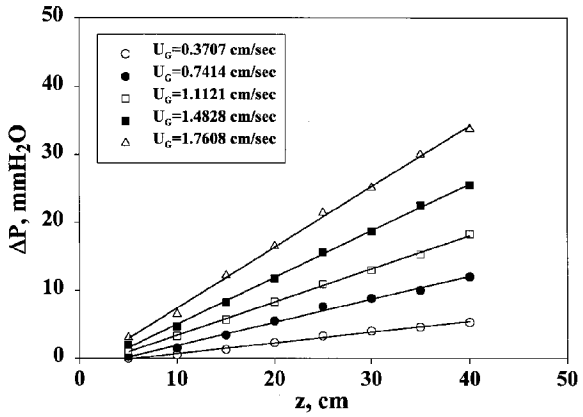

Fig. 3. Pressure variations with respect to position in a bubble column.

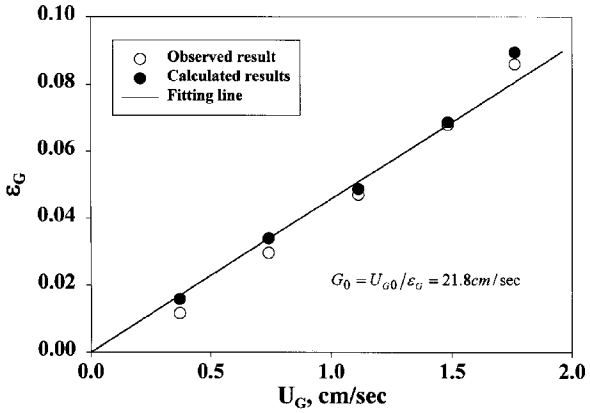

Fig. 4. Gas holdups at different U_G s in a bubble column.

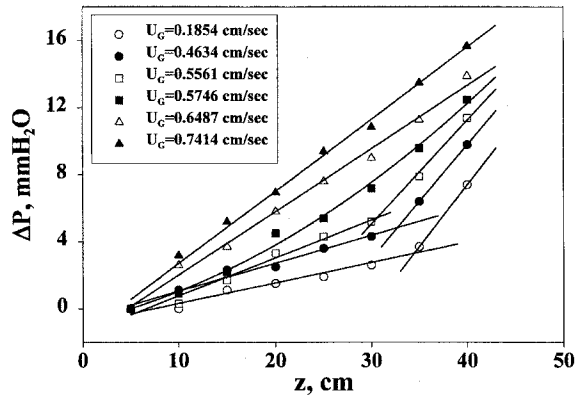

Fig. 5. Variations of the pressure profiles versus the superficial gas velocity.

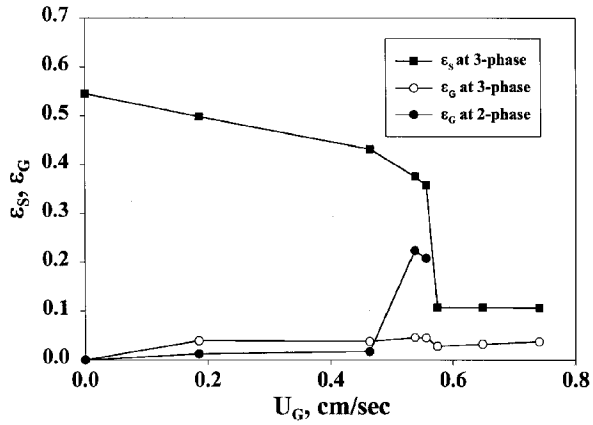

Fig. 6. Average phase holdups in the reactor with 20% particle loads.

$$\varepsilon_S=\frac{M_S}{H_b A \rho_S}. \tag{3}$$

The concentration of solids in the reactor, defined by the ratio of the static bed height to the column height, varied from 10 to 40%. The hydrodynamic behavior can be identified by the pressure profiles and the axial solid concentration profiles, when the superficial gas velocity U_G is varied. As the gas was injected, the lower portion of the bed began to be fluidized. As the gas velocity was further increased, the remaining packed portion of solid progressively moved until the entire bed was fluidized. The gas velocity at which the solid concentration was uniform throughout the bed is called the critical fluidization velocity. The critical fluidization velocity was determined in the apparatus of Fig. 1. Fig. 5 shows the variations of the pressure profiles versus the superficial gas velocity and the average phase holdups in the reactor with 20% particle loading. The average phase holdups in Fig. 6 were obtained from the slopes of the lines in Fig. 5 and the previous three equations. As shown in Fig. 6, the gas phase holdups in the 2-phase region suddenly increase just before fluidization starts, while the gas phase holdups for the 3-phase region slightly decrease at the critical fluidization point. The change of the critical fluidization velocity with respect to particle loading and

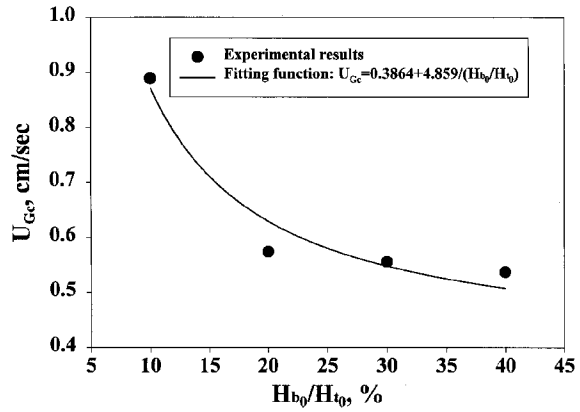

Fig. 7. Changes of the gas velocity with respect to particle loads.

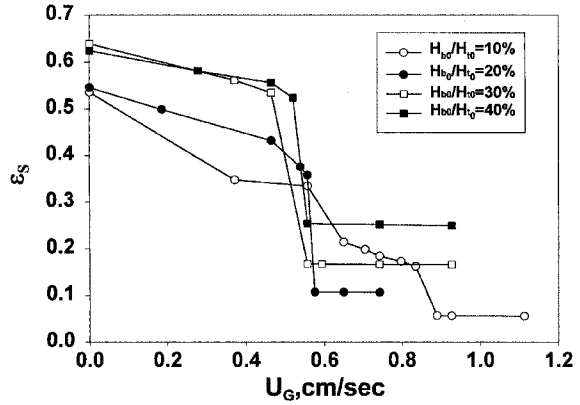

Fig. 8. Variations of the solid holdup profiles with the gas velocity.

the variations of the solid holdup profiles with the gas velocity are presented in Figs. 7 and 8, respectively. The gas velocity for the critical fluidization decreases with increasing solid particle loading. Fig. 8 shows that a gradual transition to fluidization at low particle loading is observed while a sharp transition is observed at high particle loading. This phenomenon may be explained by the percolation theory for the phase transition [Choi et al., 1995]. Our sparger shows similar performance with the rubber membrane sparger studied by others [Comte et al., 1997].

We have tried to fit our experimental data to Comte et al.'s model. The main assumption of their model is that the axial solid distribution in the column is mainly controlled by the difference between the density of the particle and that of the gas-liquid mixture which can be considered as a homogeneous fluid. The density of this mixture can be estimated as follows everywhere in the reactor whatever the conditions are:

$$\bar{\rho}=\frac{\varepsilon_G\rho_G+\varepsilon_L\rho_L}{\varepsilon_G+\varepsilon_L}. \tag{4}$$

Since the density of gas is much less than the density of liquid, Eq. (4) can be simplified by

$$\bar{\rho}=\frac{\varepsilon_L\rho_L}{\varepsilon_G+\varepsilon_L}. \tag{5}$$

If the density of solid particles is greater than the density of a gas-liquid mixture, particles will settle down to the bottom of the reactor. If the density of solid particles is less than the density of the mixture, particles will go upward. When the density of the solid particles is equal to the density of the mixture, particles will disperse in the reactor. In this model, however, the liquid circulation due to the rising gas bubbles is not considered. When the gas velocity is equal to the critical fluidization velocity, the density of the mixture equals the density of the solid particles. That is,

$$\bar{\rho}=\rho_S \tag{6}$$

and Eq. (5) becomes

$$\frac{\rho_S}{\rho_L}=\frac{\varepsilon_L}{\varepsilon_G+\varepsilon_L}. \tag{7}$$

If we define R as

$$R\equiv \frac{\rho_L-\rho_S}{\rho_L}=1-\frac{\rho_S}{\rho_L} \tag{8}$$

and combine Eqs. (2), (7) and (8), we have

$$\varepsilon_L=(1-\varepsilon_S)\frac{\rho_S}{\rho_L} \tag{9}$$

and

$$\varepsilon_G=R(1-\varepsilon_S). \tag{10}$$

From the concept of the slip velocity G defined by Wallis [1969],

$$G=\frac{U_{Gc}}{\varepsilon_G}, \tag{11}$$

the critical velocity can be expressed as follows:

$$U_{Gc}=GR(1-\varepsilon_S). \tag{12}$$

Since ρ_S=0.93 g/cm^3 and ρ_L=1.00 g/cm^3, R becomes 0.07 in our experiment. As shown in Fig. 9, G is between 8.57 and 14.29 cm/sec. When ε_S> 0.1, G is between 8.57 and 11.43 cm/s. It has been reported that solids promote bubble coalescence when G is greater than 25 cm/sec and the particles act as a 'decelerator' slowing down the rising bubbles when G is less than 25 cm/sec [Hebrard et al., 1996; Hyndman and Guy, 1995].

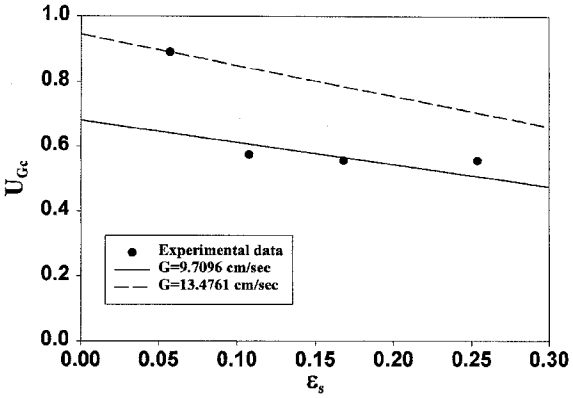

Fig. 9. Variations of the gas velocity with solid holdup.

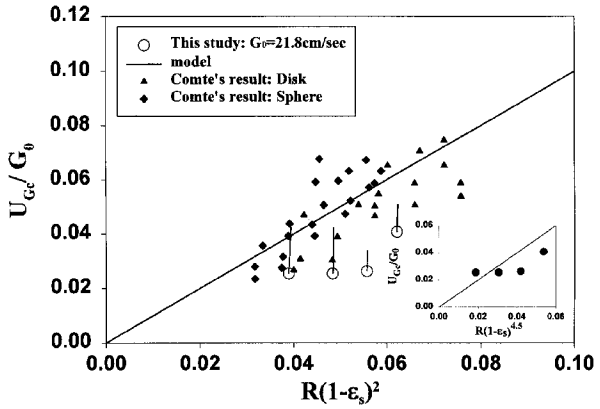

Fig. 10. Comparison of predicted values with experimental data.

Thus, it can be seen that our ceramic membrane diffuser generates small bubbles and the polymer particles decelerate. In this plot, when the solid hold-up is small such as (ε_S=0.1), the particles do not sufficiently decelerate the velocity of the rising bubbles. This means the slip velocity G depends on the presence of solids. Thus, G can be expressed as the following empirical law:

$$G=G_0(1-\varepsilon_S)^x \tag{13}$$

Since the slip velocity, G_0, is the average free rising bubble velocity, G_0=21.8 cm/sec was obtained from the bubble column data. Eq. (12) can be written as

$$U_{Gc}=G_0R(1-\varepsilon_s)^y \tag{14}$$

Fig. 10 compares our results with Comte et al.'s results. The value of the exponent y was found to be 4.5 by a simple logarithmic fitting while the value of y was found to be 2 by Comte et al. This means that we obtain smaller critical velocity of gas bubbles than Comte et al.'s critical velocity under the same solid hold-up and density conditions. Since they used untreated polyethylene beads (hydrophobic) while we used surface modified polyethylene beads (hydrophilic), the hydrophilic surface property of particles may act as a 'decelerator' slowing down the rising bubbles.

2. Flow Characteristics in the Solid-Liquid Inverse Fluidized Reactor using Centrifugal Force

The equation for the pressure drop in the packed bed is expressed by the Ergun equation, and the inverse fluidization occurs when the pressure drop in the packed bed equals the difference between the particle buoyancy and gravitational forces [McCabe et al., 1993].

$$(\rho_L-\rho_S)(1-\varepsilon_{mf})g=\frac{150U_{Lmf}\,\mu_L(1-\varepsilon_{mf})^2}{\phi^2 d_P^2\varepsilon_{mf}^3}+\frac{1.75U_{Lmf}\,\rho_L(1-\varepsilon_{mf})}{\phi^2 d_P\varepsilon_{mf}^3}. \tag{15}$$

If we introduce a factor, α, which is the relative contribution of downward flow to rotating flow, the liquid velocity for the minimum fluidization, U_{Lmf}, can be represented by the critical rotating velocity, N_{mf}.

$$U_{Lmf}=\alpha\pi N_{mf}D_a. \tag{16}$$

The balance equation for the minimum fluidization can be

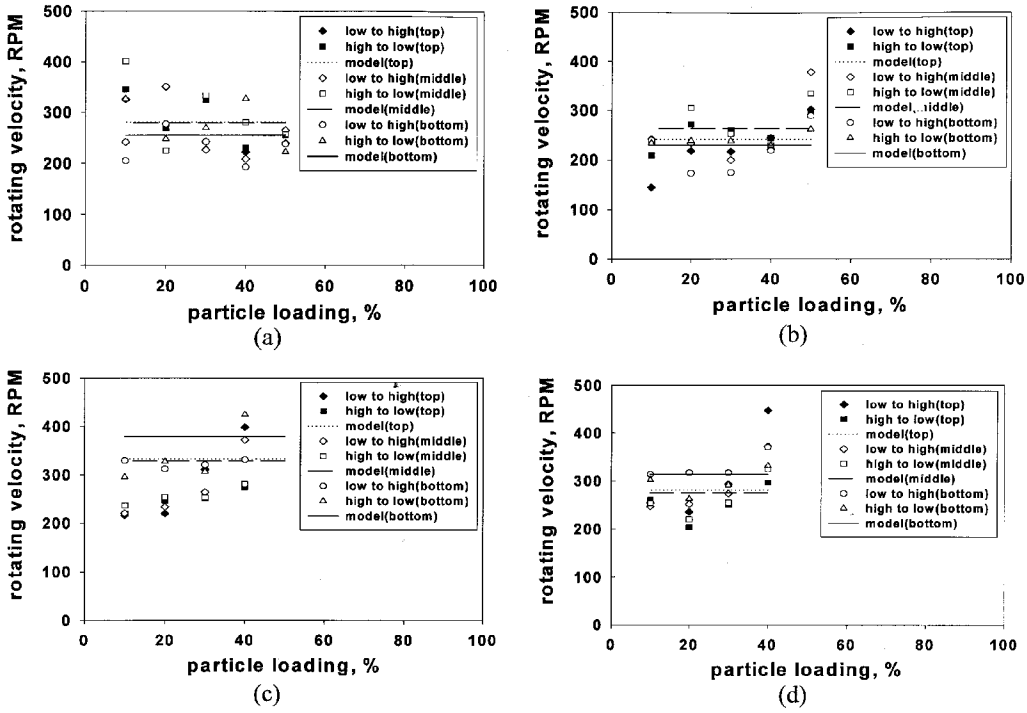

Fig. 11. Change of critical rotating velocities with respect to particle loads.
(a) untreated LDPE beads without inner tube; (b) treated LDPE beads without inner tube; (c) untreated LDPE beads with inner tube; (d) treated LDPE beads with inner tube.

Table 1. Values of α at different experimental conditions

Position of impeller	System without inner tube		System with inner tube	
	Untreated LDPE	Treated LDPE	Untreated LDPE	Treated LDPE
Top	0.00352	0.00409	0.00297	0.00353
Middle	0.00354	0.00374	0.00300	0.00354
Bottom	0.00388	0.00429	0.00260	0.00352

written as the following second order equation for $Re_{N,\,mf}$:

$$-\frac{\Phi K^2\varepsilon_{mf}^3}{1.75\alpha^2\pi^2}Ar_L=\frac{150K(1-\varepsilon_{mf})}{1.75\alpha\pi\Phi}Re_{N,\,mf}+Re_{N,\,mf}^2, \quad (17)$$

where $Re_{N,\,mf}=\frac{\rho_L N_{mf} D_a^2}{\mu_L}$ and $Ar_L=\frac{\rho_L(\rho_S-\rho_L)d_p^3 g}{\mu_L^2}<0$, and $K=\frac{D_a}{d_p}$.

Fig. 11 represents the critical rotating velocity of the impeller at the onset of fluidization with the change of particle loading. Fig. 11(a) and (b) are the results using untreated and treated LDPE beads in a reactor without inner tube, respectively, and (c) and (d) are the results using untreated and treated LDPE beads in a reactor with inner tube, respectively. Each figure represents the results obtained at three different positions: top, middle and bottom. As shown in Fig. 11, the critical rotating velocity slightly increases with increasing particle loads. To compare flow characteristics of four different cases, we calculate α from Eqs. (16) and (17) using the average critical rotating velocity and represented the results in Table 1. To obtain α, we first calculate the average value of rotating velocity, N_{mf}, at each experimental condition and adjust α until the value of N_{mf} predicted by Eq. (17) equals the average value of N_{mf} obtained at each experimental condition. We use the golden section method to find α. Since a large value of α means low energy cost for operating the reactor, the operation using treated LDPE beads in a reactor without inner tube is better than other operations. This is because the density of treated LDPE beads (ρ_S= 0.93 g/cm^3) is slightly larger than that of untreated LDPE (ρ_S= 0.903 g/cm^3) and the inner tube blocks outward flow from impeller to wall. Such a blocking effect of the inner tube has to be studied more for optimum design of reactor geometry. In addition, the hydrophilic surface property of chemically treated particles may provide easy operation of the reactor.

CONCLUSIONS

We investigated the hydrodynamic characteristics of two different three-phase inverse fluidized bed reactors: one using aeration and the other using centrifugal force. In the first reactor, only an upward gas flow allows floating low-density polyethylene beads to sink down into liquid phase and to be uniformly distributed over the entire column. The gas holdup data obtained in the bubble column showed good agreement with the results obtained from the direct measurement of bed expansion. The gas velocity for critical fluidization decreased with increasing particle loads. Thus, this reactor can be operated at low gas velocity with high load of particles. This means high population of microbes attached on the carrier surface. The slip velocity obtained from the bubble column data used to estimate the exponent of power law expression for the slip ve-

locity in the three-phase inverse-fluidized bed. The slip velocity of the three phase inverse fluidized reactor was 9.7 to 13.5 cm/sec. The predicted exponent for the power law expression of the critical velocity was 4.5 while it was 2 in Comte et al.'s study. This is because of the hydrophilic surface property of LDPE which may act as a 'decelerator' for the rising bubbles. In the second reactor, the particle loads did not highly affect the critical rotating velocity for homogeneous fluidization while the geometry of reactor spacing and the type of impeller were more important for easy fluidization. Therefore, the inverse fluidized bed reactor using aeration is more promising for the application of wastewater treatment than that using centrifugal force. However, if we combined two concepts of inverse fluidization, we could design a better reactor for effective treatment of industrial wastewater.

ACKNOWLEDGEMENTS

This work was supported by the National Special Project Corporation of Chungnam National University and Korea Microbial Technology, Inc. in 1998. Useful comments by Dr. Lee, Dong-Hyun at the University of British Columbia are greatly acknowledged.

NOMENCLATURE

A : cross section area of the column [L^2]
Ar_L : Archimedes number [dimensionless]
D_a : diameter of impeller [L]
$-d_p/dz$: axial pressure gradient [$MT^{-2}L^{-2}$]
d_p : particle diameter [L]
g : gravitational acceleration [LT^{-2}]
G : slip velcity [LT^{-1}]
G_0 : slip velocity for ε_S=0 [LT^{-1}]
H_b : bed height [L]
K : constant for the ratio of D_a to d_P [dimensionless]
M_S : weight of solid introduced into the column [M]
N_{mf} : rotating velocity for minimum fluidization [T^{-1}]
$R=1-\rho_S/\rho_L$: density ratio [dimensionless]
$Re_{N,\,mf}$: Reynolds number for minimum fluidization [dimensionless]
U_{Lmf} : liquid velocity for the fluidization [LT^{-1}]
U_{GC} : critical gas velocity [LT^{-1}]
x, y : exponent in Eqs. (13) and (14) [dimensionless]

Greek Letters

α : relative contribution of downward flow to rotating flow [dimensionless]
ε_{mf} : porosity at minimum fluidization [dimensionless]
ε_G : gas holdup [dimensionless]
ε_L : liquid holdup [dimensionless]
ε_S : solid holdup [dimensionless]
$\bar{\rho}$: gas-liquid mixture density [ML^{-3}]
ρ_G : gas density [ML^{-3}]
ρ_L : liquid density [ML^{-3}]
ρ_S : solid density [ML^{-3}]
μ_L : viscosity of liquid water [$ML^{-1}T^{-1}$]
Φ : sphericity of particle [dimensionless]

REFERENCES

Bastoul, D., Roustan, M., Capdeville, B. and Audic, J. M., "Multiphase Reactors for Biological Treatment of Urban Wastewaters," In Environmental Technologies and Trends, Produserv Verlagservice, Berlin, 183 (1996).

Choi, H. S., Talbot, J., Tarjus, G. and Viot, P., "Percolation and Structural Properties of Particle Deposits," Physical Review E., **51**, 1353 (1995).

Comte, M. P., Bastoul, D., Hebrard, G., Roustan, M. and Lazarova, V., "Hydroynamics of a Three-phase Fluidized Bed-The Inverse Turbulent Bed," *Chem. Eng. Sci.*, **52**, 3971 (1997).

Dibyendu, S., Bag, V., Pradeep, K. and Sukamar, M., "Etching of a Low-density Polyethylene Film by Fuming Nitric Acid," *Die Aangewandte Makromorekulate Chemic*, 249 (1997).

Fan, L. S., Muroyama, K. and Chern, S. H., "Hydrodynamic Characteristics of Inverse Fluidization in Liquid-Solid and Gas-Liquid-Solid Systems," *Chem. Eng. J.*, **24**, 143 (1982).

Frieda, Dr. and Kolot, B., "Microbial Carriers Strategy for Selection," *Process Biochemistry*, Aug/Sept., 2 (1981).

Hebrard, G., Bastoul, D. and Roustan, M., "Influence on the Gas Sparger on the Hydrodynamics of a Bubble Column," *Trans. IchemE A-74*, 406 (1996).

Hihn, J. Y., Gonthier, Y. and Bernis, A., "Le lit fluidis triphasique inverse fonctionnant contre courant de gaz et de liquide: hydrodynamique et transfert de matire," *Rec. Prog. En Genie des Proc.*, **6**, 11 (1992).

Hyndman, C. L. and Guy, C., "Gas Phase Hydrodynamics in Bubble Columns," *Int. Chem. Engng*, **73**, 302 (1995).

Koh, J. S. and Chang, H. N., "Anaerobic Treatment of MSG Waste with CSTR and Filter," *HWAHAK KONGHAK*, **17**, 281 (1979).

Krishnaiah, K., Guru, S. and Sekar, V., "Hydrodynamic Studies on Inverse Gas Liquid Solid Fluidization," *Chem. Eng. J.*, **51**, 109 (1993).

Lee, C. W., Choi, H. S., Park, Y. T. and Doh, K. S., "The Characteristics of Hydrodynamics and Mass Transfer in Three Phase Fluidized Column with Draft Tube," *HWAHAK KONGHAK*, **27**, 472 (1989).

Lee, S. L. P. and De Lasa, H. I., "Phase Holdups in Three Phase Fluidized Beds," *AIChE J.*, **33**, 1359 (1987).

Legile, P., Menard, C., Laurent, C., Thomas, D. and Bernis, A., "Contribution a l'etude hydrodynamique d'un lit fluidis triphasique inverse fonctionnant contre courant," *Entropie*, **143**, 11 (1988).

McCabe, W. L., Smith, J. C. and Harriott, P., "Unit Operations of Chemical Engineering 5th ed.," McGraw-Hill, New York (1993).

Nikolov, L. and Karamanev, D., "Experimental Study of the Inverse Fluidized Bed Biofilm Reactor," *Can. J. of Chem. Eng.*, **65**, 214 (1987).

Roustan, M., Bastoul, D. and Capdeville, B., "Influence of the Hydrodynamic Behavirour of a Three Phase Fluidized Bed for Effluent Treatment. 3rd;" Int. Conf. on Bioreactor and Bioprocess Fluid Dynamics, Cambridge, UK (1993).

Wallis, G., "One-Dimensional Two Phase Flow," McGraw-Hill, New York (1969).

Wild, G., Saberian, M., Schwartz, J. L. and Charpentier, J. C., "Les racteurs lits fluidises gas-liquide-solide. Etat de l'art et perspectives industrielles," *Enrtopie*, **106**, 3 (1982).
Yang, D. C., Kim, J. H. and Yoo, Y. J., "Development of Support by Chemical Modification for the Immobilization of Activated Sludge," *HWAHAK KONGHAK*, **35**, 129 (1997).
Yoon, H. H., Ghim, Y. S., Chang, H. N., Kim, Y. J. and Rhee, J. S., "Wastewater Treatment Using a Dual Biological Reactor System," *HWAKHAK KONGHAK*, **20**, 293 (1982).